atmosphere

MDPI

Article

Contrasting Impacts of ENSO on the Interannual Variations of Summer Runoff between the Upper and Mid-Lower Reaches of the Yangtze River

Xiaochen Ye [1] and Zhiwei Wu [2,3,*]

[1] Earth System Modeling Center and Key Laboratory of Meteorological Disaster of Ministry of Education, Nanjing University of Information Sciences & Technology, Nanjing 210044, China; yxc@nuist.edu.cn
[2] Department of Atmospheric and Oceanic Sciences & Institute of Atmospheric Sciences, Fudan University, Shanghai 200438, China
[3] Shanghai Key Laboratory of Meteorology and Health, Shanghai 200030, China
* Correspondence: zhiweiwu@fudan.edu.cn

Received: 9 September 2018; Accepted: 3 December 2018; Published: 5 December 2018

Abstract: The Yangtze River Basin is an El Niño–Southern Oscillation (ENSO)-sensitive region, prone to floods and droughts. Hydrological records were collected to examine the temporal and spatial distribution of runoff in this drainage basin. An apparent difference in runoff variations between the upper and mid-lower Yangtze reaches was detected in response to ENSO. The upper basin usually experiences floods or droughts during the summer of ENSO developing years, while the mid-lower runoff variations tend to coincide with ENSO decaying phases. Composite analysis is employed to investigate the underlying mechanism for the teleconnection between the specific phases of the ENSO cycle and Yangtze runoff variation. Results show that the Western Pacific Subtropical High (WPSH) exhibits large variability on its western side in summer with different ENSO phases, thus resulting in a contrasting influence between the upper and mid-lower Yangtze floods and droughts. During the central Pacific-La Niña developing summers, the WPSH is significantly enhanced with its westward extension over the Yangtze upper basin. Anomalous water vapor converges in its northwest edge thus favoring upper-basin flooding. Meanwhile, the mid-lower reaches are controlled by the WPSH, and the local rainfall is not obvious. In addition, when the El Niño decaying phases occur, the WPSH denotes a westward extending trend and the position of its ridge line shifts to the mid-lower Yangtze reaches. The southwest moisture cannot extend to the upper basin but converges in the mid-lower basin. Accompanied by the anomalous 100 hPa South Asia High and lower-tropospheric Philippines anticyclone movements, this upper–middle–lower configuration acts as a key bridge linking ENSO and Yangtze floods and droughts.

Keywords: Yangtze River runoff; ENSO cycle; WPSH; interannual variations

1. Introduction

The Yangtze River (YR), being a major link among the world's highest plateau (Qinghai–Tibet Plateau), largest continent (Eurasia) and largest ocean (the Pacific), is of utmost importance in terms of water resources transportation and circulation. However, in recent decades, more frequent flood hazards and waterlogging disasters struck the YR Basin, causing serious economic losses. Flood records showed that in the summer of 1954 and 1998, the entire Yangtze drainage area suffered from tremendous flooding [1–3]. Besides flood events, long-lasting wet and drought conditions in the YR Basin have also inflicted considerable impacts on the local ecological environment and human society over the region [4,5]. YR Basin is a hydroclimatically-sensitive region [6] so that the singularities of the large-scale atmospheric circulation could help predict extreme floods and droughts occurrence [7,8].

Therefore, identifying the connections between meteorological change (e.g., the Tibetan Snow Cover, East Asian summer monsoon (EASM), etc.) and frequent drought and flood events has been the main focus of hydrometeorological research in the YR Basin.

The El Niño–Southern Oscillation (ENSO) has been recognized as the most pronounced interannual oscillation signal of the climate system [9], interacting and coupling between ocean and atmosphere. It not only directly causes the weather and climate anomalies in the tropical area, but also affects weather conditions outside the tropical Pacific even global climate by teleconnection. Former scholars indicated that Sea Surface Temperature (SST) anomalies of the equatorial Pacific show a profound influence on summer climate in East Asia [10–13]. Traditional ENSO events occur on the coast of Peru along the eastern equatorial Pacific, and the SST anomaly gradually extends westward. A new type of ENSO event whose warm/cold center is developed from the central Pacific (CP) has been observed in recent years [14]. Several researches have highlighted the significance of distinguishing different episodes of SST in the Pacific when discussing the ENSO impacts [15,16], mainly considering different types of ENSO changes in the location and strength of the thermal heating from the underlying surface which may exert different influences on atmospheric circulation.

However, previous studies only aimed at illustrating the impact of ENSO's cold and warm phases on rainfall in eastern China, but seldom considered the influence of different stages of ENSO events to the Yangtze runoff. The possible influence of ENSO events on annual streamflow in the YR Basin remains complicated. Furthermore, few studies have ever tried to distinguish the contrasting impacts of ENSO to the runoff between the upper and mid-lower reaches separately, where the climatic and geographical backgrounds are quite inconsistent. Undoubtedly, a better understanding of the hydrological series variability and its physical cause in different parts of the Yangtze basin is of scientific and practical interest.

Therefore, the main objective of this paper is to investigate the contrasting impact of different phases and stages of ENSO events on the interannual variability of the upper and mid-lower Yangtze runoff and try to determine the physical cause. The manuscript is structured as follows. In Section 2, we briefly introduce the data and the study area. Then we give a description of the distinguished long-term variations and trends of upper and mid-lower runoff along the mainstream of the YR in Section 3. The connection between the ENSO cycle and the YR runoff cycle are then presented in detail in Section 4, followed by a discussion of the physical mechanism of this study in Section 5. Conclusions and discussions are listed in the final section.

2. Data and Study Area

2.1. Data

The datasets used in this study include (1) monthly Sea Surface Temperature (SST) from the Extended Reconstructed SST Version 3b (ERSST.V3b) [17] for the period of 1950–2016 collected from the National Oceanic and Atmospheric Administration (NOAA); (2) Niño1+2, Niño3, and Niño4 index calculated from the NOAA Climate Prediction Center (CPC) and defined by the averaged SST anomalies over the extreme eastern tropical Pacific (0–10° S, 80°–90° W), eastern tropical Pacific (5° S–5° N, 90–150° W), and central equatorial Pacific (5° S–5° N, 160° E–150° W), calculated by the ERSST.V3b; Niño5 and Niño6 index, namely, the additional western Pacific indices are defined as follows, Niño5 over (5° S–5° N, 120–140° E) and Niño6 over (8–16° N, 140–160° E), calculated by the ERSST.V3b [18]; (3) monthly mean 100 hPa, 500 hPa, 850 hPa winds, and corresponding geopotential height fields and sea level pressure for the period of 1950 to 2016 obtained from the National Centers for Environment Prediction/National Center for Atmospheric Research (NCEP/NCAR) reanalysis [19]; (4) monthly mean precipitation at 160 stations for the period of 1950 to 2016, provided by the National Climatic Centre of China Meteorological Administration (CMA); (5) monthly mean runoff data at three main gauging stations in the Yangtze Basin: Yichang Station, Hankou station, and Datong station for the period of 1950 to 2016. In this study, summer refers to June–July–August (JJA).

2.2. Basin Description

The YR is the longest river in China and the third longest river in the world, passing through three major economic zones in the east, central, and west of China. As illustrated in Figure 1, originating from the Qinghai–Tibet Plateau, the YR streams through eleven provinces and extends 6300 km eastward before finally flowing into the East China Sea [20]. This river basin lies between (91–122° E, 25–35° N) and covers a total drainage area of 1.81×10^6 km^2 [21]. Since the large longitudinal span of this catchment gives rise to sharp variabilities in hydroclimatic characteristics in this area, the whole Yangtze watershed area can be traditionally divided to the upper and mid-lower reaches corresponds to the altitude zones.

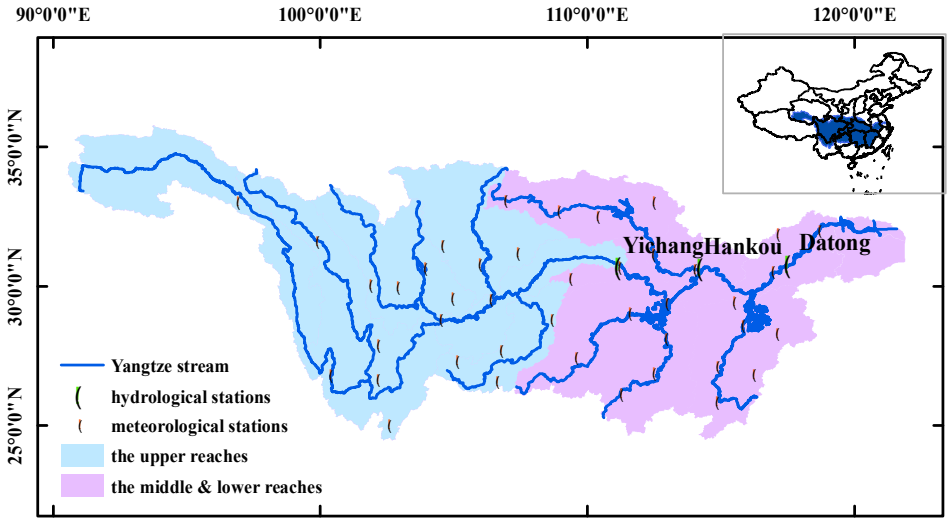

Figure 1. River networks of the Yangtze River (YR) basin. Stream gauging stations and meteorological stations are marked.

The upper YR consists of the area from the headwaters to Yichang station, which has a total drainage area of about 1×10^6 km^2, taking up 56% of the YR Basin (the blue shaded area in Figure 1). The complicated topography in the upper reaches has essential impacts on the local climate, and the spatial distribution of the precipitation is extremely uneven [22]. Apart from the great topographic variability, the upper reaches of the YR Basin are influenced by the Indian southwestern summer monsoon each year. Meanwhile, the mid-lower stream is located between Yichang and Datong stations, diverging along the surrounding tributaries to form a basin (the purple shaded area in Figure 1). The hydrological regimes of the mid-lower reaches are significantly influenced by land-sea thermal contrast and the East Asian southeastern summer monsoon, which are deemed to have great influence for the occurrences of floods and droughts here. The contrasting climates and landscapes of the upper and mid-lower basins may lead to different hydrological regimes. Therefore, the intercomparison of climate background of droughts and floods in both two basins is expected to be necessary.

3. Distinct Features of Runoff Variations in the Upper and Mid-Lower Reaches of the Yangtze River

Figure 2a illustrates the distribution of observed 67-year mean monthly runoff in the upper and mid-lower reaches of the YR Valley from 1950 to 2016. The Yangtze mainstream monthly runoff varies within a year. Mostly, the runoff of the mid-lower Yangtze reaches is concentrated in early summer from May to July (May–June–July, MJJ) in a year. However, the upstream flow is concentrated in the rainy season from July to September (July–August–September, JAS), lagging behind the mid-lower reaches for about two months. In the upper basin, runoff during the concentration period JAS could occupy 49.6% of the annual runoff on the average, and the maximum of monthly runoff appeared in July, which was 7.4 times than the minimum in February.

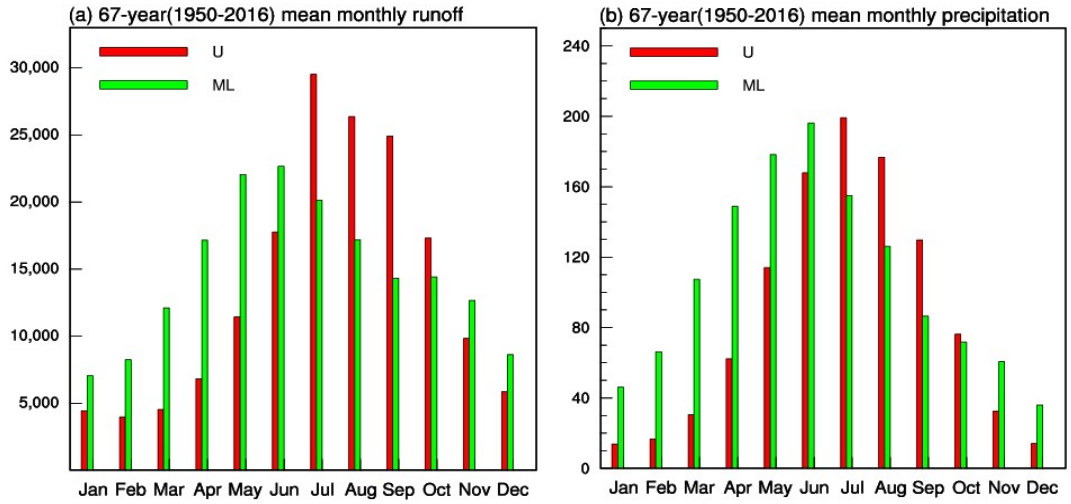

Figure 2. Distribution of observed multiyear average monthly (**a**) runoff (m^3/s) and (**b**) precipitation (mm/day) from 1950 to 2016. The red and green bars represent the upper and mid-lower reaches of the YR, respectively.

Runoff distribution in the upper and mid-lower reaches reflects contrasting patterns both spatially and temporally. It is clear that YR Basin is a hydroclimatically-sensitive region and rainfall is the main driver of intensified floods and prolonged droughts. The 67-year mean monthly watershed mean precipitation is presented separately for 12 months as bar charts in Figure 2b. Results show that rainfall in the upper Yangtze valley mainly concentrated in June to August and in May to July for the mid-lower reaches. The precipitation concentration period in the upper reaches is also lagged behind that in the mid-lower reaches. The different annual distribution of precipitation and runoff in the upper and lower reaches of the Yangtze River Basin is probably a result of the seasonal migration of the major rainband from the southeast to northwest China during the warm season.

Given that floods and droughts are more likely to occur during the concentration period, we studied the upper and mid-lower runoff during their concentration period, which is more valuable for flood forecasting. Normalized runoff time series of the upper (JAS) and mid-lower (MJJ) reaches measured over 1950 to 2016 were examined using simple linear regression and Mann–Kendall (MK) trend test to identify the long-term trends (Figure 3). A significant downward trend at the 95% confidence level was found in the upstream flood-season streamflow variations, while no obvious trend was detected for summer runoff change in the mid-lower YR during 1950 to 2016 based on the MK test. The temporal variation of both upper and mid-lower Yangtze runoff exhibits significant variability on the interannual timescale.

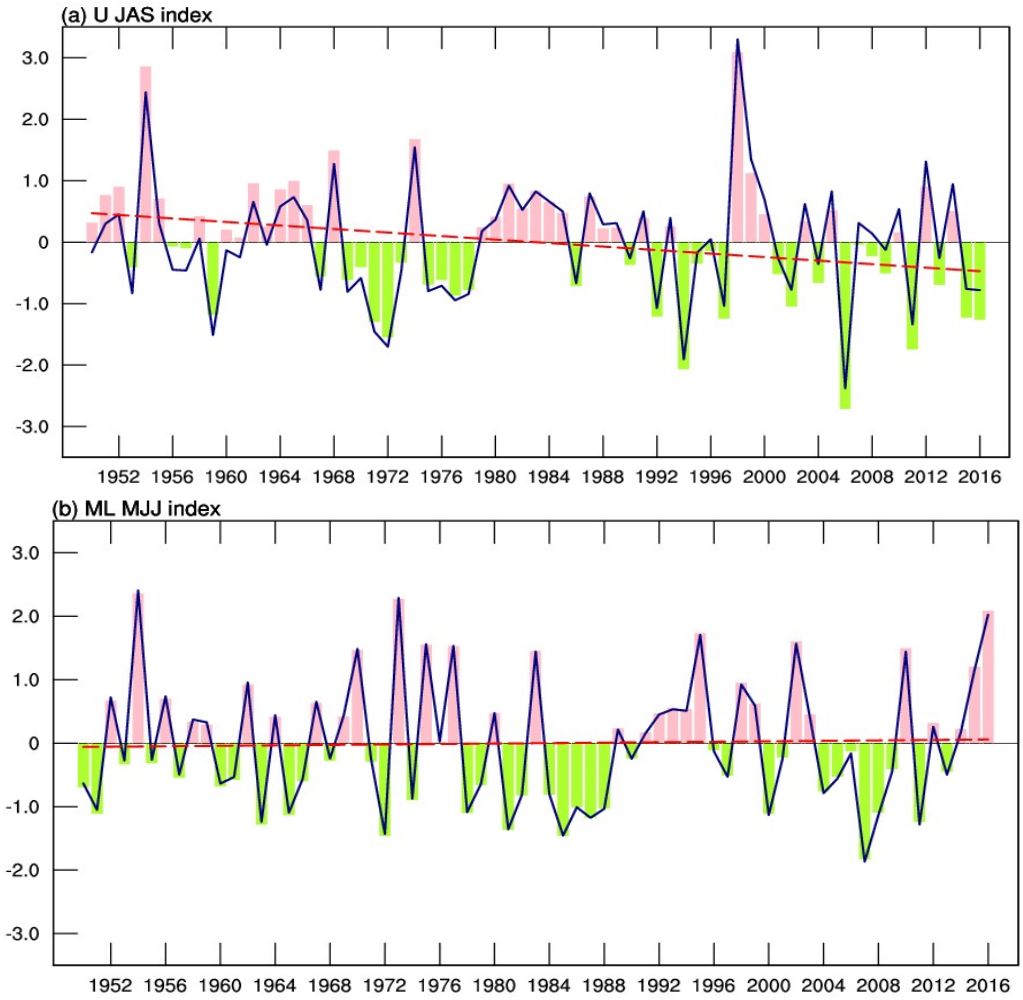

Figure 3. Time series of normalized observed runoff (bars) and detrended runoff (blue curves) in each concentration period at the (**a**) upper (U) and (**b**) mid-lower (ML) reaches of the YR, respectively. Red lines represent the trend. In this study, MJJ means May–June–July and JAS means July–August–September.

We define the detrended runoff time series (blue curves in Figure 3) value > 0.9 (<−0.9) standard deviation as the criterion to obtain the years of remarkably runoff anomaly for the following composite analysis. Based on this metric, eight wetter years (1998, 1954, 1974, 1999, 2012, 1968, 2014, and 1981) and nine drier years (2006, 1994, 1972, 1959, 1971, 2011, 1992, 1997, and 1977) are picked out for the 1950 to 2016 period in the upper reaches. For the mid-lower reaches, there are thirteen wetter years (1954, 1973, 2016, 1995, 2002, 1975, 1977, 1970, 1983, 2010, 2015, 1962 and 1998) and fourteen drier years (2007, 1985, 1972, 1981, 2011, 1963, 1987, 2008, 2000, 1965, 1978, 1951, 1988, and 1986).

4. ENSO Cycle and the Yangtze River Runoff Cycle

Figure 4 displays the composite differences of SST anomaly patterns between the greater and lesser runoff years selected above (more minus less) in the upper YR. A negative anomaly develops rapidly from the previous winter to subsequent autumn, relating to an ENSO developing phase. In the developing summer, marked negative SST anomalies are located over the central equatorial Pacific with maximum SST anomalies centered over the west of 150° W, accompanied by weak warm SST anomalies over the extratropical western Pacific. For the mid-lower reaches, a large-scale positive SST anomaly covers the eastern to central tropical Pacific in the prior winter, which has been weakening from winter to the succeeding summer (Figure 5) in linkage with an ENSO decaying phase. There is no

minimal SST anomaly over the equatorial central-eastern Pacific in the summertime. A faint negative SST anomaly appears until the following autumn, which seems to have a tendency to transform to a La Nina-like pattern.

The lead–lag correlation coefficients between the Niño3, Niño4 index (representing the key area of the ENSO cycle), and upper, mid-lower runoff time series from JJA (−1) to JJA (1) are shown in Figure 6. Here, "−1" denotes the previous year, number "0" signifies this year, and number "1" represents the succeeding year. Mostly, the upper Yangtze runoff indicates an intimate negative connection with the Niño4 index in JJA (0), and the correlation with the Niño3 index does not turn significant until September-October-November (SON) (0). Such a close relationship persists to D (0) JF (1) (dashed curve in Figure 6a), which suggests that the upper runoff is normally related to CP–ENSO developing phases. That is to say, floods and droughts of the upper reaches tend to occur in the CP–ENSO developing summer. However, the mid-lower Yangtze runoff appears to have a decreasingly correlation with the Niño3 and Niño4 index since the preceding D (−1) JF (0) and both the correlation coefficient reaches the maximum in the D (−1) JF (0), which indicates that the mid-lower runoff is related to the decaying phase of ENSO. As a supplement, we also calculated the lead–lag correlation coefficients between the Niño1+2, Niño5, and Niño6 indices [18] and upper, mid-lower runoff time series. Together, all these indices can fully represent the whole picture of ENSO events. We found that the upper Yangtze River runoff time series shows significant connection with Niño1+2, Niño5, and Niño6 indices during SON (0) or D (0) JF (1), while the mid-lower runoff time series is significantly related to the Niño1+2 index from SON (−1) to D (−1) JF (0) and Niño6 from D (−1) JF (0) to March-April-May (MAM) (0). In general, the correlation between ENSO and runoff is a carbon copy of the result of the composite analysis. Namely, the upper runoff is associated with an ENSO developing phase, whereas the mid-lower runoff is related to an ENSO decaying phase.

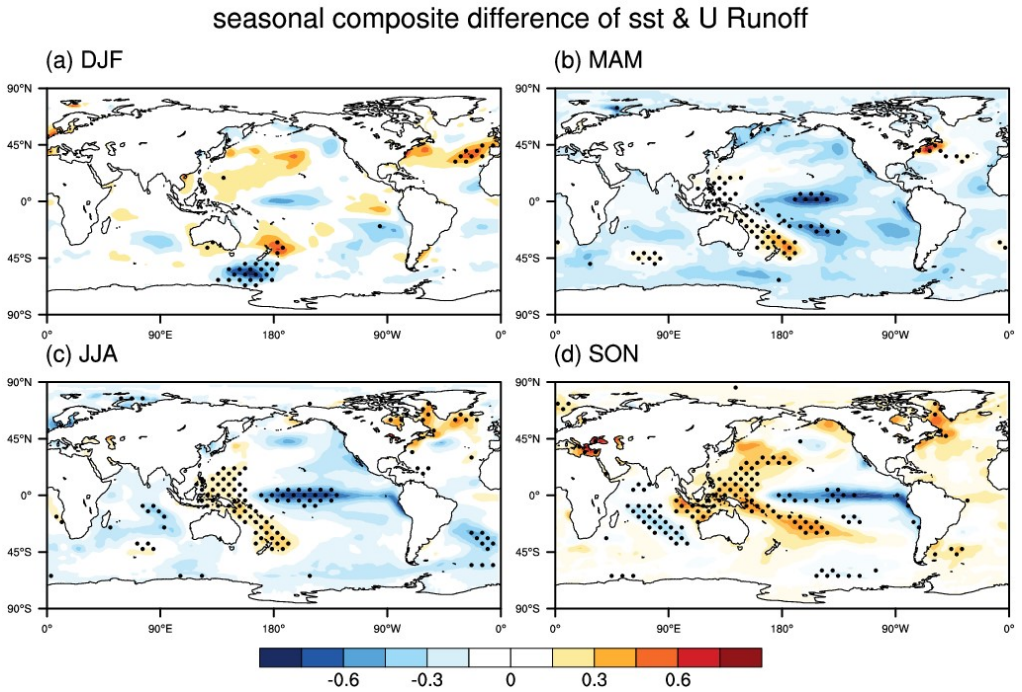

Figure 4. The composite difference of Sea surface temperature (SST) from the previous winter to autumn. (high—low upper July–August–September (JAS) runoff years; color shadings). Black dots are statistically significant at the 95% confidence level on the basis of a Student's *t*-test. In this study, DJF means December-January-February, MAM means March-April-May, JJA means June-July-August and SON means September-October-November.

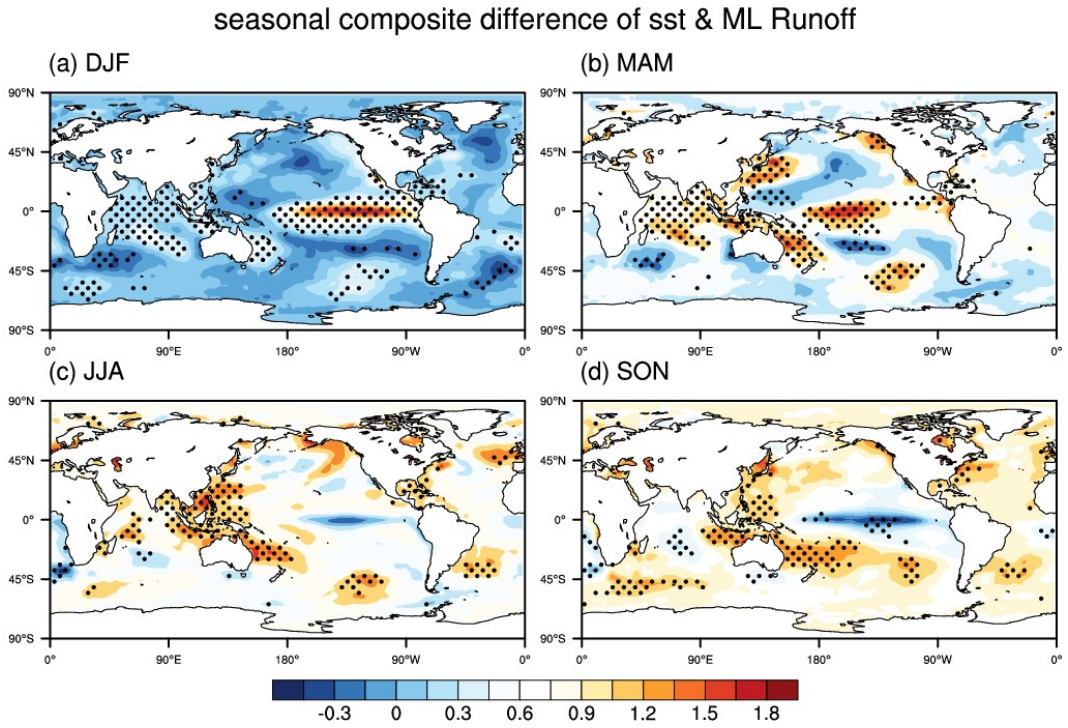

Figure 5. Same as Figure 4 but for the mid-lower May–June–July (MJJ) runoff years.

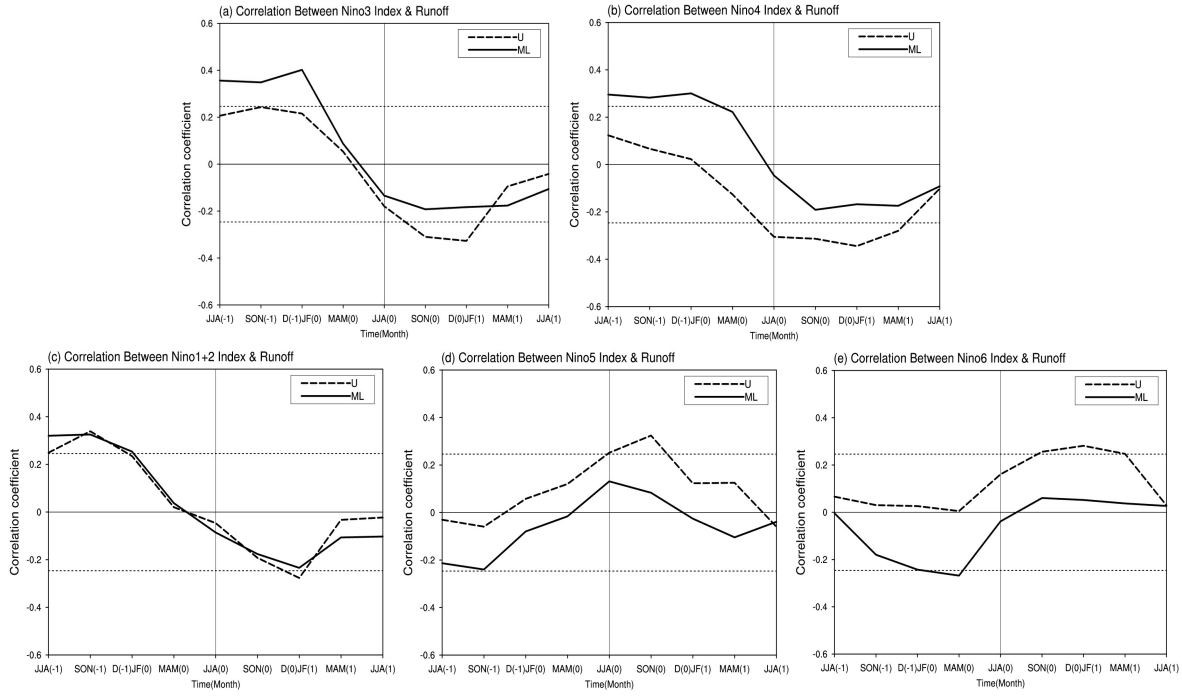

Figure 6. The lead–lag correlation coefficients between the upper and mid-lower reaches runoff time series in Figure 3 and the (**a**) Niño3, (**b**) Niño4, (**c**) Niño1+2, (**d**) Niño5, and (**e**) Niño6 indices from June–July–August (JJA) (−1) to JJA (1). The two horizontal lines represent the 95% confidence level based on Student's *t*-test. The vertical line indicates JJA (0), where the simultaneous correlations between the two runoff series and El Niño–Southern Oscillation (ENSO) indices are shown.

5. Physical Mechanism

5.1. Classification of ENSO Types

Due to the phase-locking nature of ENSO, ENSO events generally peak during the boreal winter, persist into spring and fade by the following summer in an annual cycle [23]. The corresponding atmospheric anomaly response to different ENSO phases is different, and its climate impacts are also different. Many studies have confirmed that the impact of ENSO events on year to year climate anomalies is closely related to what stage they are in. Therefore, we adopted the CPC's definition to select the representative years of typical ENSO events. That is, if the Niño3.4 index values (calculated by three months running mean, covering the region 5° S–5° N, 120–170° W) are higher than 0.5 °C or less than −0.5 °C for five consecutive months, this year will be categorized as an El Niño (La Niña) year. In this way, we picked twenty-two El Niño events and fourteen La Niña events from 1950 to 2016 (Table 1). We regard the beginning year of an event as the development stage and the end year of an event as the attenuation stage.

Table 1. Years dominated by different ENSO events during 1950–2016.

El Niño
1951/1952,1953 */1954,1957/1958,1958/1959,1963 */1964,1965 */1966,1968/1969,1969/1970,1972/1973,1976/1977,1977 */1978,1979/1980,1982/1983,1986/1987 */1988,1991/1992,1994 */1995,1997/1998,2002 */2003,2004/2005,2006/2007,2009/2010,2014/2015/2016
La Niña
1950/1951,1954/1955/1956,1964/1965,1967/1968,1970/1971/1972,1973/1974,1974/1975 */1976,1984/1985,1988 */1989,1995/1996,1998 */1999/2000/2001,2007/2008,2010 */2011,2011/2012,2016 */2017

Note. '*' represent CP-El Niño and CP-Niña years.

However, when ENSO events occur, the corresponding climatic responses are quite sensitive to the meridional migration and intensity of equatorial Pacific SST anomalies. Traditional ENSO has positive or negative SST anomalies center in the equatorial Pacific cold tongue region, yet CP–ENSO is typically characterized by anomalous warm or cold water center over the central equatorial Pacific. Consistently, the canonical Eastern Pacific (EP) ENSO and CP–ENSO can be identified according to the zonal locations of SST anomalies. Several studies have provided a variety of indexes to define ENSO events. Cao [24] argued the Niño3 index could represent the EP–El Niño pattern effectively and the Niño4 index is skillful in separating the CP–El Niño events. However, for the existence of asymmetry of ENSO, the warm events are not completely contrary to the cold events. In other words, La Niña events cannot be considered to be the opposite sign of El Niño events. For seasonal prediction, particularly, treating ENSO events as linear systems will miss some vital signals. Ren and Jin [25] proposed new Niño indices by simply transforming Niño3 and Niño4 indices; these indices help characterize the zonal propagation of SST warm anomalies but fail to separate the La Niña events in to two categories. In addition, Zhang et al. [26] explained that in spite of the fact that their index is skillful in identifying EP- and CP–El Niño, it is not suitable for distinguishing La Niña events. Accordingly, the classification of two types of ENSO, typically the La Niña events, requires taking the Niño indices together with the SST anomalies distribution into account [27–29]. However, in current studies, researchers identify the CP and EP events mainly based on the mature stage of La Nina.

In this study, we select ENSO events referring to the CPC's definition of ENSO events combining the SST anomaly pattern in the summer period. Events having abnormal summer SST distribution centered in the west of 150° W are classified as the CP–El Niño and CP–La Niña (CP–ENSO) developing events. Those years characterized by westward-propagating SST anomalies which have two anomaly centers in both east and west of 150° W, which are confusing to tell apart in terms of air–sea coupling characters and have been excluded in the following work. The selected events are marked in Table 1. Seven CP–El Niño and five CP–La Niña developing summers were identified, which is largely consistent with the classification in former research [26,29].

5.2. Associated Atmospheric Responses

Given that the runoff variations in the upper and mid-lower reaches of the YR are closely allied to ENSO, the composite method is synthesized to reveal the summer atmospheric responses to developing/decaying or warm/cold phases of ENSO. The intensity and location of the South Asia high in summer are crucial systems that affect the climate anomalies in the eastern position of the Tibetan plateau [30–32]. Figure 7a denotes the composite features of JJA 100 hPa geopotential height field among the CP–La Niña developing summers selected above, using Student's two-tailed significance test. The blue curves represent the combination of the climatologically averaged JJA geopotential height with the corresponding anomalies, in other words, the real situation field. It can be seen that the region around the vicinity of 20° N to 40° N, which is covered by the main body of South Asian high (SAH), is a zone that is all positively anomalous (as indicated by shades in Figure 7a, passing the 95% or 90% confidence level of the *t*-test). The SAH is obviously enhanced, expanding eastward and lifting northward and can strengthen the upper-level divergence and low-level convective motion over the Yangtze upper basin, which is favorable for maintaining the lower-level Western Pacific Subtropical High (WPSH) in a northward and westward position (Figure 7b). Based on the distribution pattern of 100 hPa geopotential height field from June to August among the El Niño decaying years (Figure 8a), the SAH has a simultaneous eastward shift, which is cooperating with the slightly westward 500 hPa WPSH (Figure 8b). The significant positive anomaly appears in the regions east of around 90° E, but the anomaly position is a bit southward. This finding is in accord with the connection between the WPSH and the SAH proposed by Tao and Zhu [33].

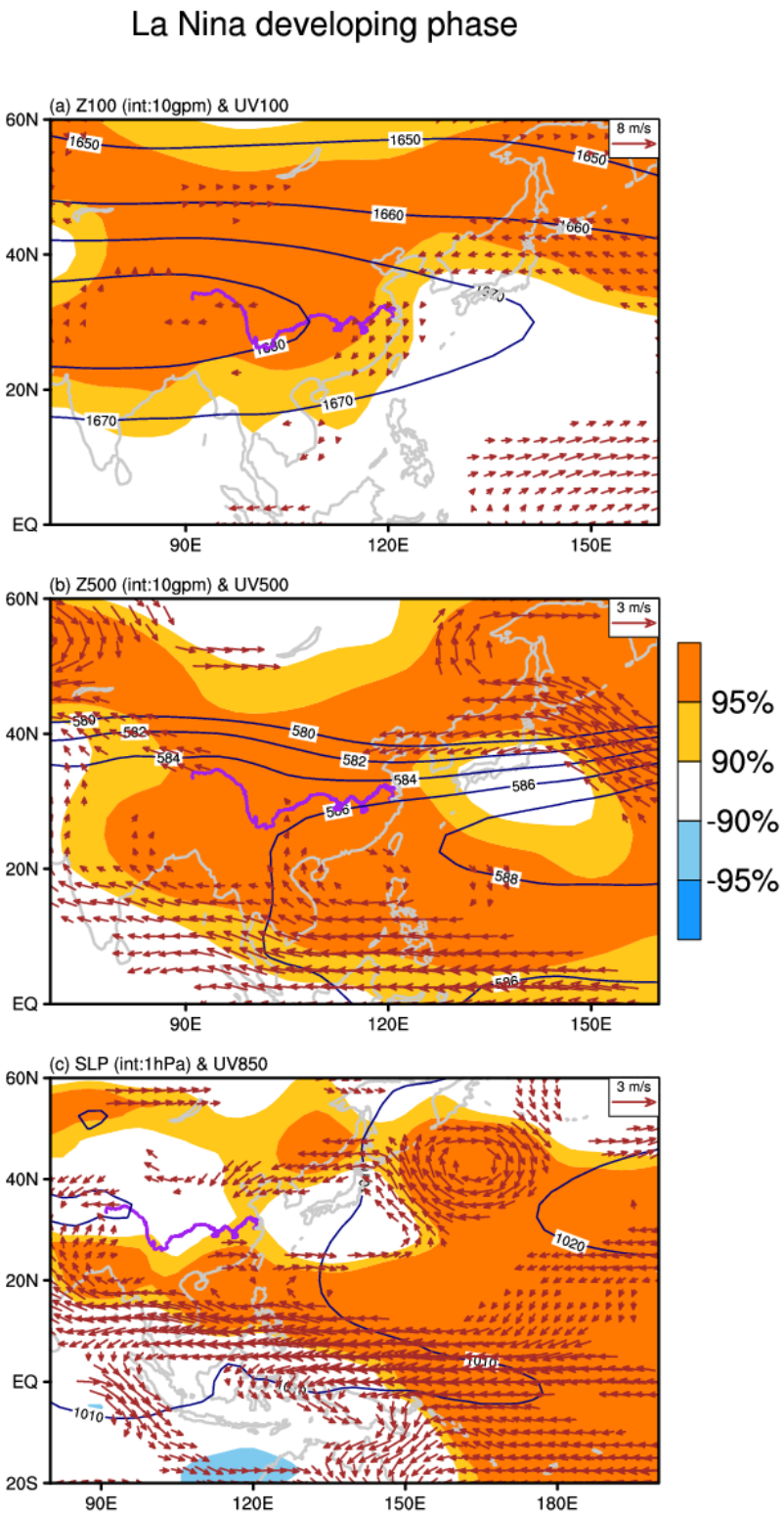

Figure 7. The JJA composite of the 100 hPa and 500 hPa geopotential height fields, sea level pressure (Z200, Z500, and SLP), and wind (UV200, UV500, and UV850) in the CP–La Niña developing phase from 1950 to 2016. The blue contours represent the climatological mean of JJA Z200, Z500, and SLP plus the corresponding anomalies, that is, the real condition. The shadings indicate the areas beyond 95% and 90% confidence level based on a Student's *t*-test). Arrows denote the UV200, UV500, and UV850, and only those data points statistically significant over the 90% confidence level are drawn.

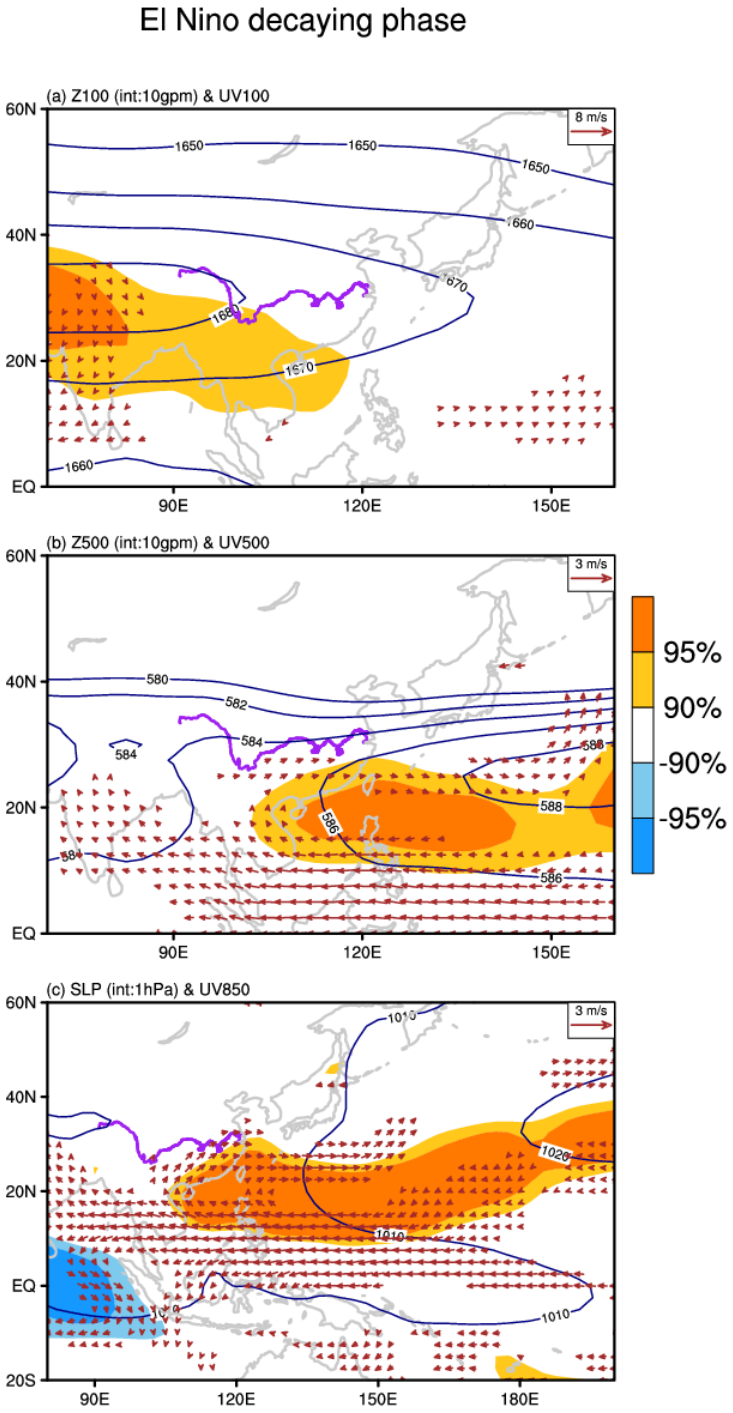

Figure 8. Same as Figure 7, but for the El Niño decaying phase.

Additionally, the convection anomaly over the Pacific associated with ENSO can also influence the mid-latitude pattern. The West Pacific subtropical high is the main circulation system directly affecting the summer rainfall in China. During CP–La Niña developing summers, East Asia and the surrounding sea exhibit a distribution pattern that is positively anomalous. The WPSH (Figure 7b) is shifted far further westward than the climatological average, and the western frontier of the 586 potential height (10 gpm) contour line stretches to the west of 105° E, and its ridge (105° to 110° E) lies between 27.5° N and 30° N. The Yangtze upstream is located in the northwest edge of the subtropical high. As a result, a large amount of warm and humid flow from the western North Pacific is transported westward to the upper YR Basin, and meets the cold and dry flow from the north here, which is conducive to

the development of rainfall. At the same time, the mid-lower reaches are under the control of the subtropical high, and the precipitation is decreased. While in El Niño decaying summers, the WPSH is shifted slightly southwestward, and the westernmost ridge point of the 586-10 gpm geopotential meter line is situated west of 117° E, as shown in Figure 8b. Consequently, moisture from the western North Pacific is delivered to the mid-lower YR Basin, which is just at the northwest side of the WPSH. The westward shift of the WPSH during the decaying ENSO summers will cause the occurrence of the second period of Meiyu and increase rainfall [1]. However, compared to the CP–La Niña developing summers, the El Niño decaying summers experienced weaker western or southwestern wind and anticyclone. This may explain why the water vapor transport cannot reach the upper reaches, but land in the mid-lower reaches. These conclusions are consistent with the results about 100 hPa.

For the lower-troposphere anomalies, 850 hPa wind variability can affect water vapor transportation from western tropical Pacific to the subtropical region, further influencing the runoff over the Yangtze basin. Figures 7 and 8 display the common characteristics of ENSO-related composite 850 hPa wind anomalies and sea level pressure (SLP). In terms of CP–La Niña developing and El Niño decaying-related SST variations, the anomalous SLP displays an apparent positive anomaly in the western equatorial Pacific during JJA. Meanwhile, the low-level easterly anomaly prevails around the equatorial oceanic regions from the Indian Ocean to the western Pacific. In consequence, anomalous airflow diverged and settled over the western equatorial Pacific, forming an anomalous anticyclone around the Philippines, namely, the Philippines anticyclone (PA).

Former research has determined that the PA provides a key circulation system which conveys ENSO influence to climatic change in East Asia [28], mainly focusing on the explanation of the formation mechanism of the anticyclone and how the ENSO anomalies (mature in the prior winter) develop and persist to exert cross-seasonal influences after their mature phases from boreal winter to the ensuring early summer [34]. Wang et al. [35,36] interpreted that this anticyclone develops rapidly in the prior winter and, owing to the positive local air–sea thermodynamic feedback between Rossby waves and the underlying warm pool ocean around the Philippine Sea, the anticyclone is maintained from the previous winter to the following summer. They also pointed out that the developing of this anticyclone is almost coincident with the enhancement of the local sea surface cooling. Xie et al. [37] emphasize the role of the Indian Ocean, which stores the ENSO signal in the previous winter and releases it in the summer like a capacitor that causes the PA anomaly in the summer by stimulating the eastward Kelvin fluctuations.

Compared with the El Niño decaying phase, the SLP positive anomalies related to the CP-La Niña developing events shift far westward and a little bit northward. Along with the SLP anomalies, it is noticeable that the PA is westward- and slightly northward-shifted, partly owing to the westward displacement of the SST anomaly center. To the northwest flank of this anomalous anticyclone are anomalous southwesterly winds along the surrounding regions. These anomalous winds substantially bring plentiful moisture to this region. Anomalous southwesterly wind prevails over the upper YR Basin, which brings further vapor transport over this area. Note that U_{850}, V_{850}, and SLP anomaly intensity and spatial scale are weaker and smaller during the El Niño decaying summers than during the CP–La Niña developing events. This is partially attributed to the PA trace can be searched back to prior winter [35,36] when significant westerly wind anomalies appear around the equatorial eastern Pacific region in ENSO decaying years; this signal is not so noticeable in the flowing summer. The anomalous southwesterly along the anticyclone will dominate southeastern Asia, triggering largely increased runoff in the mid-lower Yangtze reaches. In addition, both the anticyclone and the cooling region propagate slowly eastward [34,38]. It explains, to a certain extent, why the ENSO decaying phase only affects the mid-lower runoff.

During the El Niño developing and La Niña decaying summers, however, the low-level wind anomalies over the western North Pacific reverse sign. A weak anomalous cyclone emerges in the western north Pacific region. The 500 hPa subtropical high is obviously located more eastward

than normal, which weakened the transportation of moisture in eastern China and caused reduced precipitation, thus causing dry conditions along the YR Basin.

6. Conclusions and Discussion

Extraordinary floods and droughts are usually attributed to unique atmospheric circulation patterns in connection with climatic change. The hydrological system in the YR Basin is very sensitive to ENSO. The upstream floods in the YR correspond to the development phase of ENSO cold events, while the mid-lower reaches tend to be linked with the attenuation of ENSO warm events.

The large-scale circulation background of the different ENSO phases impacting the Yangtze runoff has pronounced differences in summer. At high level, the SAH is generally enhanced with its northward advance and eastward extension over the region east of the Plateau, which is favorable for lower-level WPSH to be maintained in a northward and westward position. Compared with the developing phase, however, the anomaly is slightly southward and eastward during the decaying phase. At mid-level, the West Pacific Subtropical High shows large variability on its western side in summer. It is shifted westward to the upper and mid-lower YR Basin, separately, during developing and decaying phases, which exerts significant contrasting influence to the regional runoff change by moisture from the western North Pacific, which is transported to its west-north edge. For lower latitude, note that in summertime, a prominent feature—a simultaneous low-level anticyclone circulation—is apparently located in the western north Pacific as pointed out by Wang et al. [35,36]. In the northwestern part of the anticyclone, anomalous southerlies and southwesterly winds tend to bring more vapor transport. However, all the atmosphere response is weaker during the El Niño decaying summers than during the CP–La Niña developing summers, partly due to that is not so significant in the flowing summer of ENSO decaying years. Furthermore, it can be seen that the teleconnections between ENSO and Yangtze runoff are very sensitive to the zonal locations of the tropical Pacific warming/cooling. The anticyclone moves slowly eastward over time as pointed by Wu et al. [13], Chou [34], and Chen [38]. It explains, to a certain extent, why the ENSO developing phase can exert impact on Yangtze River upstream but the ENSO decaying phase only affects the mid-lower runoff. These findings suggest that ENSO might provide a prominent indicator for seasonal wetness and drought forecast in the YR Basin. Increasing attention should be paid to the cause of the occurrence of floods and droughts, thus serving for sustainability and hydro-environmental protection in this region.

Moreover, runoff in the upper YR Basin was featured by a distinct decreasing trend. The magnitude of the runoff variations was relatively small over the mid-lower YR valley (Figure 3). Like the trend observed for runoff, precipitation in the upper basin tended to decrease in the past 67 years. Annual rainfall signified no obvious trend in the mid-lower reaches of the YR. That is to say, in addition to an interannual cycle, Yangtze runoff also experiences a marked interdecadal variation and the difference between the interdecadal changes in the upstream and the mid-lower reaches remains poorly understood. Subsequently, the current findings focus on the relationship of ENSO with YR runoff, and we may conduct a further investigation to analyze the importance of Tibetan Plateau heating, Eurasian snow cover, and polar ice coverage as well. In addition to climate change effects, intensive human activities (e.g., irrigation, dam construction, etc.) are believed to have impact on hydrological processes in recent decades, whose cause also needs to be uncovered.

Author Contributions: Formal analysis, X.Y. and Z.W.; Writing—Original draft, X.Y.; Writing—Rreview & Editing, Z.W.

Funding: This work was jointly supported by the National Natural Science Foundation of China (NSFC) [41790475], the National Key Research & Development Program of China [2016YFA0601801], the Ministry of Science and Technology of China [2015CB453201 and 2015CB953904], and the NSFC [91637312, 41575075 and 91437216].

Conflicts of Interest: The authors declare no conflicts of interest.

References

1. Tao, S.; Zhang, Q.; Zhang, S. The great floods in the Changjiang River valley in 1998. *Clim. Environ. Res.* **1998**, *3*, 291–298.
2. Yang, Y.; Wei, Z. Comparison and consideration of the Yangtze River flomp in 1998 and 1954. *Meteorol. Sci. Technol.* **1999**, *1*, 16–19.
3. Zong, Y.; Chen, X. The 1998 flood on the Yangtze, China. *Nat. Hazards* **2000**, *22*, 165–184. [CrossRef]
4. Xu, J.; He, Q.; Liu, H.; Chen, J. Preliminary analysis of characteristics of the exception allow discharge and its cause over the Yangtze River, 2006. *Resour. Environ. Yangtze Basin* **2008**, *5*, 716–722.
5. Ma, J. Revelation and countermeasures of catastrophic drought disasters in recent years in Southwest China. *Yangtze River* **2010**, *41*, 7–12.
6. Ye, X.; Wu, Z.; Wang, Z.; Shen, H.; Xu, J. Seasonal prediction of the Yangtze River runoff using a partial least squares regression model. *Atmos. Ocean* **2018**, *56*, 117–128. [CrossRef]
7. Wu, Z.; Li, J.; He, J.; Jiang, Z. Large-scale atmospheric singularities and summer long-cycle droughts-floods abrupt alternation in the middle and lower reaches of the Yangtze River. *Sci. Bull.* **2006**, *51*, 2027–2034. [CrossRef]
8. Wu, Z.; Li, J.; He, J.; Jiang, Z. Occurrence of droughts and floods during the normal monsoons in the mid and lower reaches of the Yangtze River. *Geophys. Res. Lett.* **2006**, *33*, L05813. [CrossRef]
9. Webster, P.; Magana, V.; Palmer, T.; Tomas, T.; Ma, Y.; Yasunari, T. Monsoons: Processes, predictability, and prospects for prediction. *J. Geophys. Res.* **1998**, *103*, 451–510. [CrossRef]
10. Huang, R.; Wu, Y. The influence of ENSO on the summer climate change in china and its mechanism. *Adv. Atmos. Sci.* **1989**, *6*, 21–32.
11. Zhang, R.; Sumi, A.; Kimoto, M. A diagnostic study of the impact of El Niño on the precipitation in China. *Adv. Atmos. Sci.* **1999**, *16*, 229–241. [CrossRef]
12. Feng, S.; Hu, Q. Variations in the teleconnection of ENSO and summer rainfall in northern China: A role of the Indian summer monsoon. *J. Clim.* **2003**, *17*, 4871–4881. [CrossRef]
13. Wu, R.; Hu, Z.; Kirtman, B. Evolution of ENSO-related rainfall anomalies in East Asia. *J. Clim.* **2003**, *16*, 3742–3758. [CrossRef]
14. Kao, H.; Yu, J. Contrasting Eastern-Pacific and Central-Pacific types of ENSO. *J. Clim.* **2009**, *22*, 615–632. [CrossRef]
15. Zhang, W.; Jin, F.; Turner, A. Increasing autumn drought over southern china associated with ENSO regime shift. *Geophys. Res. Lett.* **2014**, *41*, 4020–4026. [CrossRef]
16. Zhang, L.; Wu, Z.; Zhou, Y. Different impacts of typical and atypical ENSO on the Indian summer rainfall: ENSO-developing phase. *Atmos. Ocean* **2016**, *54*, 440–456. [CrossRef]
17. Smith, T.; Reynolds, R.; Peterson, T.; Lawrimore, J. Improvements to NOAA's historical merged land-ocean surface temperature analysis (1880–2006). *J. Clim.* **2008**, *21*, 2283–2296. [CrossRef]
18. Wang, C.; Robert, H.; Jyotika, I. Western Pacific interannual variability associated with the El Niño-Southern Oscillation. *J. Geophys. Res.* **1999**, *104*, 5131–5149. [CrossRef]
19. Kalnay, E.; Kanamitsu, M.; Kistler, R.; Collins, W.; Deaven, D.; Gandin, L.; Zhu, Y. The NCEP/NCAR 40-year reanalysis project. *Bull. Am. Meteorol. Soc.* **1996**, *77*, 437–471. [CrossRef]
20. Chen, Z.; Zhao, Y. Impact on the Yangtze (Changjiang) Estuary from its drainage basin: Sediment load and discharge. *Chin. Sci. Bull.* **2001**, *46*, 73–80. [CrossRef]
21. Zhang, Q.; Liu, C.; Xu, C.; Xu, Y.; Jiang, T. Observed trends of annual maximum water level and streamflow during past 130 years in the Yangtze River basin, China. *J. Hydrol.* **2006**, *324*, 255–265. [CrossRef]
22. Zhang, Q.; Jiang, T.; Gemmer, M.; Becker, S. Precipitation, temperature and runoff analysis from 1950 to 2002 in the Yangtze basin, China. *Int. Assoc. Sci. Hydrol. Bull.* **2005**, *50*, 26–27.
23. Wang, B. Interdecadal changes in El Niño onset in the last four decades. *J. Clim.* **1995**, *8*, 267–285. [CrossRef]
24. Cao, L. Two Types of ENSO and Atmospheric Circulation Responses. Master's Dissertation, Department of Atmospheric Sciences, Nanjing University, Nanjing, China, 2011.
25. Ren, H.; Jin, F. Niño indices for two types of ENSO. *Geophys. Res. Lett.* **2011**, *38*, L04704. [CrossRef]
26. Zhang, W.; Wang, L.; Xiang, B.; Li, Q.; He, J. Impacts of two types of La Niña on the NAO during boreal winter. *Clim. Dyn.* **2015**, *44*, 1351–1366. [CrossRef]

27. Yeh, S.; Kug, J.; Dewitte, B.; Kwon, M.; Kirtman, B.; Jin, F. El Niño in a changing climate. *Nature* **2009**, *461*, 511–514. [CrossRef] [PubMed]
28. Yuan, Y.; Yan, H. Different types of La Niña events and different responses of the tropical atmosphere. *Chin. Sci. Bull.* **2012**, *57*, 3312–3322. [CrossRef]
29. Wang, L.; Zhang, W.; Qi, L.; He, J. Contrasting air-sea features associated with two types of La Niña during the seasonal evolution. *Acta Oceanol. Sin.* **2014**, *36*, 72–85. [CrossRef]
30. Li, Y. Analysis of 100 hpa circulation variation and the drought flood anomalies in Sichuan province and Chongqing city. *J. Chengdu Inst. Meteorol.* **1999**, *1*, 8–13.
31. Luo, S.; Qian, Z.; Wang, Q. The weather investigation on the relation between 100 hPa South Asia High in summer and the drought and flood in the east of China. *Plateau Meteorol.* **1982**, *1*, 1–10.
32. Chen, Y.; Li, Y.; Qi, D. The analysis on effect of South Asia High in mid-summer extreme drought and flood years of Sichuan-Chongqing regions. *J. Trop. Meteorol.* **2012**, *28*, 924–932.
33. Tao, S.; Zhu, F. The 100-mb flow patterns in southern Asia in summer and its relation to the advance and retreat of the West-Pacific subtropical anticyclone over the Far East. *Acta Meteorol. Sin.* **1964**, *34*, 385–395.
34. Chou, C. Establishment of the low-level wind anomalies over the western North Pacific during ENSO development. *J. Clim.* **2004**, *17*, 2195–2212. [CrossRef]
35. Wang, B.; Zhang, Q. Pacific-East Asian teleconnection. part II: How the Philippine sea anomalous anticyclone is established during El Niño development. *J. Clim.* **2002**, *15*, 3252–3265. [CrossRef]
36. Wang, B.; Wu, R.; Fu, X. Pacific–East Asian teleconnection: How does ENSO affect East Asian climate? *J. Clim.* **1999**, *13*, 1517–1536. [CrossRef]
37. Xie, S.; Hu, K.; Hafner, J.; Tokinaga, H.; Du, Y.; Huang, G.; Sampe, T. Indian ocean capacitor effect on indo-western pacific climate during the summer following El Niño. *J. Clim.* **2009**, *22*, 730–747. [CrossRef]
38. Chen, J.; Li, T.; Shih, C. Fall persistence barrier of sea surface temperature in the South China Sea associated with ENSO. *J. Clim.* **2007**, *20*, 158–172. [CrossRef]